MITOR: Jurnal Teknik Elektro

Design and Simulation of Bridgeless Cuk Converter as Electric Vehicle Battery Charger

Demas Sabatino[1,*], Mohd Ashraf Ahmad[2]
Fakultas Teknik Elektronika dan Komputer – Universitas Kristen Satya Wacana[1]
Faculty of Electrical and Electronics Engineering Technology – Universiti Malaysia Pahang Al-Sultan Abdullah[2]
Salatiga, Indonesia[1]; Pahang, Malaysia[2]
*demas.sabatino@uksw.edu

Abstract – *Two-wheeled electric vehicles in Indonesia have special specifications with SNI standards for rechargeable battery components. To recharge the battery using a household PLN power source, a charger device is required that meets both the input and output specifications. In this study, a battery charger device is designed and simulated with an output voltage specification of 72 V and a maximum current of 3 A. The charger uses a bridgeless Cuk converter topology with an input voltage of 220 V_{rms} AC household electricity. Based on the input and output specifications, the design calculation yields a nominal duty cycle of 18.8% at a switching frequency of 100 kHz, and component values of $L_1 = 5.61$ mH, $L_2 = 1.3$ mH, $C_1 = 736.3$ nF, and $C_{out} = 781$ nF. The first simulation with a fixed duty cycle of 18.8% produces a full-wave sinusoidal output signal with a peak voltage of -70.5 V, average voltage of -45 V, peak current of -2.93 A, and average current of -1.87 A. The power efficiency in this simulation is 96.2%. The second simulation introduces a duty cycle control using a comparator comparing a sawtooth waveform with the Cuk converter output. This approach yields a more stable output with a peak voltage of -100 V, average voltage of -73 V, peak current of -4 A, and average current of -3.05 A. The power efficiency in this case reaches 96.99%.*

Keywords – *Bridgeless Cuk Converter; Battery Charger; Electric Vehicle; Duty Cycle Control; Power Efficiency.*

I. INTRODUCTION

VARIOUS battery specifications for various electronic applications will always require a suitable charging device, even though the power outlet provided by PLN has a voltage of 220 Vac. Therefore, it is necessary to rectify and step down the voltage to produce a suitable power supply device.

In a linear power supply, the AC voltage is first stepped down using a transformer, then rectified with a diode. The drawbacks of this method are the bulky size of the power supply and its low power efficiency. To overcome this, a switching mode power supply (SMPS) was introduced, which rectifies the PLN voltage using a diode and then steps down the voltage using a DC-DC converter.

DC-DC converters have various basic topologies such as buck, boost, buck-boost, flyback, Cuk, and so on. Each topology has different characteristics and is used for different applications. DC-DC converters come in various topologies, each with distinct characteristics suited for different applications. The basic topologies include buck, boost, buck-boost, Cuk, SEPIC, and flyback converters [1, 2]. These converters can step up or step down voltage levels, with efficiency approaching 100% [2]. Buck converters are suitable for inductive loads like motors, while boost converters increase voltage [1, 3]. Advanced topologies incorporate switched inductor/capacitor, voltage multiplier, and magnetic coupling techniques to improve power density and boost ability [4]. DC-DC converters are crucial in solar PV systems for maximum power point tracking [5]. The choice of topology depends on factors such as efficiency, cost, and application requirements [6]. Recent developments focus on extended voltage range converters for renewable energy and electric vehicle applications [7].

However, they all require an electronic switch, typically a MOSFET or IGBT, driven by a pulse input to regulate the output voltage. Due to its high efficiency and compact component size, the DC-DC converter is widely applied in many applications, including battery

The manuscript was received on May 5, 2025, revised on June 26, 2025, and published online on July 25, 2025. Emitor is a Journal of Electrical Engineering at Universitas Muhammadiyah Surakarta with ISSN (Print) 1411 – 8890 and ISSN (Online) 2541 – 4518, holding Sinta 3 accreditation. It is accessible at https://journals2.ums.ac.id/index.php/emitor/index.

charging systems.

Rechargeable batteries play a vital role in the electric vehicle ecosystem because they provide the energy source for driving electric motors. Rechargeable batteries, particularly lithium-ion batteries, are crucial for electric vehicles (EVs) due to their high energy density, efficiency, and long cycle life [8, 9]. These batteries power the electric motors and auxiliary systems in EVs, offering advantages over traditional fossil fuel vehicles in terms of emissions reduction and energy independence [10, 11]. Battery management systems are essential for optimizing performance, safety, and longevity [8, 12]. While lithium-ion batteries currently dominate the EV market, research continues on alternative technologies such as magnesium and sodium-ion batteries [13]. Advancements in battery materials, cell architecture, and solid-state designs aim to improve safety, cost-effectiveness, and charging speeds [14, 15]. These developments are crucial for the widespread adoption of EVs and the transition to sustainable transportation. To design a DC-DC converter for battery charging applications, it is essential to know the battery specifications. In Indonesia, electric motorbike batteries—particularly those designed to be swappable—are standardized by the Indonesian National Standard (SNI), with a nominal voltage of 72 V, a nominal voltage range of 67–78 V, and a minimum energy capacity of 1300 Wh [16].

In this study, the battery charger will use PLN electricity as the input, applying a bridgeless Cuk converter topology to improve power conversion efficiency and reduce conduction losses.

Despite the wide adoption of DC-DC converters, existing research often focuses on ideal conditions or isolated topologies without considering practical input sources such as single-phase AC from PLN and specific national standards like SNI 8928:2023. This leaves a gap in designing converters that align with real-world electric vehicle charging requirements in Indonesia.

Therefore, the objective of this study is to design and simulate a battery charger using a bridgeless Cuk converter, tailored to the SNI-standard swappable battery for electric motorcycles. The converter is expected to produce an output of 72 V and 3 A with high efficiency, while also evaluating two control methods—fixed and feedback-based duty cycle—in simulation.

II. Research Methods

This study employs a simulation-based approach to analyze the performance of a battery charging system using a bridgeless Cuk converter topology. The design process begins with examining the fundamental characteristics of the converter, followed by determining the appropriate component values based on the target specifications. The simulation is then conducted under two scenarios: with a fixed duty cycle and with a feedback-controlled duty cycle.

To understand the difference between the conventional and bridgeless configurations, Figure 1 illustrates the AC to DC converter using the conventional Cuk topology with a diode bridge rectifier (DBR), while Figure 2 shows the configuration without the DBR, which is referred to as the bridgeless Cuk topology.

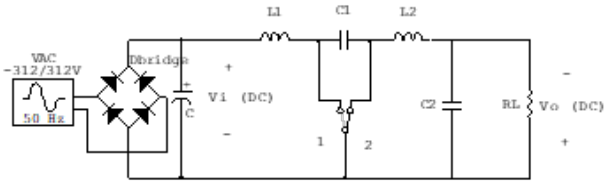

Figure 1: AC to DC converter using Cuk topology with diode bridge (DBR) as rectifier.

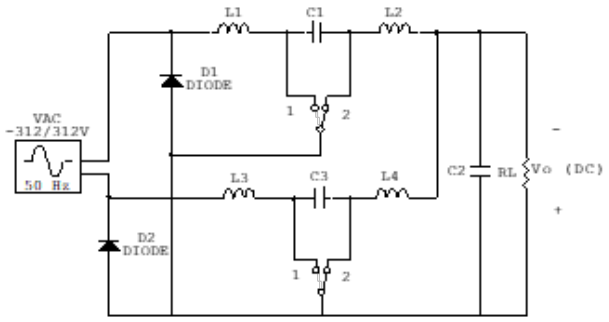

Figure 2: AC to DC converter using diode bridgeless (DBR-less) Cuk topology.

i. Bridgeless Cuk Converter

The Cuk Converter is a development of the buck-boost converter, where its advantage lies in the continuous input and output currents [17, 18], thus reducing the occurrence of electromagnetic interference noise (EMI). Because the Cuk converter is fundamentally a DC-DC converter, the AC voltage source from PLN must first be rectified. One rectification method is to use a diode bridge (DBR), as illustrated previously in Figure 1.

However, to improve the power factor of the circuit, a Cuk converter topology was developed without using DBR, referred to as the bridgeless Cuk converter [19–22], as shown in Figure 2.

The converter operates in four switching cycles, which are depicted in Figure 3. These cycles are described assuming all passive components initially have zero stored energy.

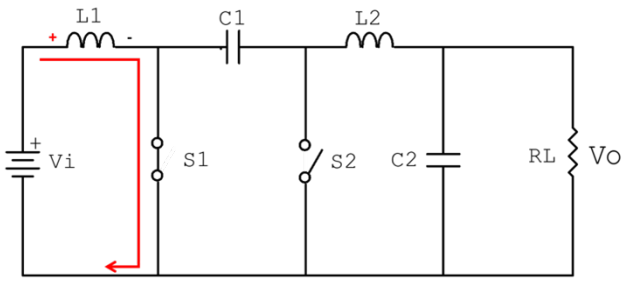

(a)

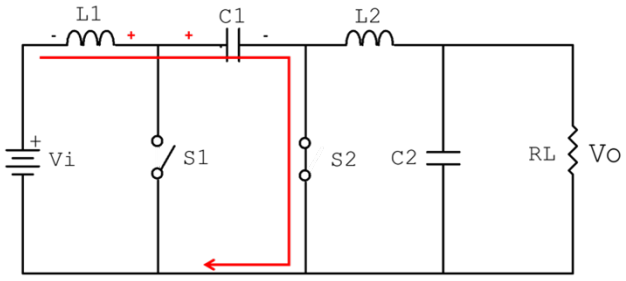

(b)

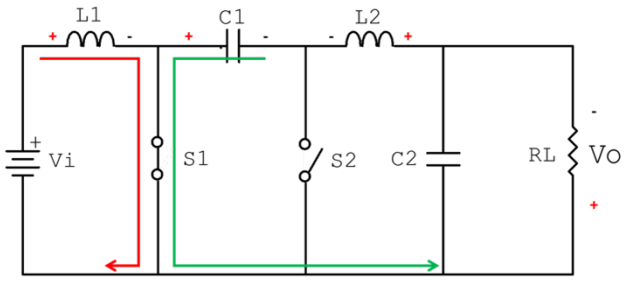

(c)

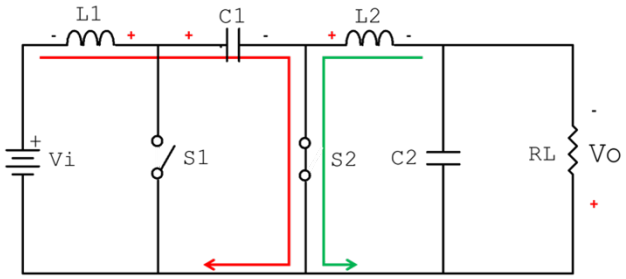

(d)

Figure 3: Cuk converter cycle assuming the initial condition of all passive components is zero: (a) first cycle of charging L_1; (b) second cycle of charging C_1; (c) third cycle of charging L_1, L_2 and discharging C_1; (d) fourth cycle of charging C_1 and discharging L_2.

ii. Switching Cycle

The Cuk converter essentially operates with two complementary switches, S_1 and S_2, as shown in Figure 3(a) [23]. When the converter is initially powered on and all passive components are assumed to have zero initial conditions, the first switching cycle begins. In this first cycle, S_1 is turned on while S_2 is off, allowing the current to flow through the closed loop $V_I \rightarrow L_1 \rightarrow S_1$, as illustrated in Figure 3(a). In the second cycle, S_1 is off and S_2 is on, resulting in capacitor C_1 being charged via the closed loop $V_I \rightarrow L_1 \rightarrow C_1 \rightarrow S_2$, as shown in Figure 3(b). During the third cycle, S_1 is on and S_2 is off, the current continues to flow through $V_I \rightarrow L_1 \rightarrow S_1$. Since C_1 is now charged, it begins discharging through $C_2 \rightarrow L_2 \rightarrow C_1 \rightarrow S_1$, as illustrated in Figure 3(c). In the fourth cycle, S_1 is turned off and S_2 is on again, repeating the charging of C_1 via $V_I \rightarrow L_1 \rightarrow C_1 \rightarrow S_2$, and discharging L_2 through the path $C_2 \rightarrow L_2$, as shown in Figure 3(d). After these four stages, the converter enters a steady-state operation where the third and fourth cycles repeat continuously. This switching principle is also applied in the Bridgeless Cuk Converter, an example of which is depicted in Figure 4, showing the current path during the positive half-cycle of the AC input voltage.

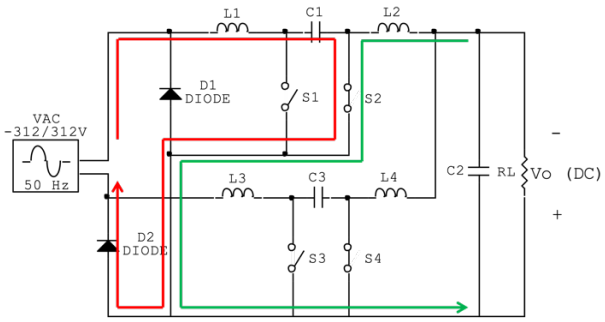

Figure 4: Current direction in the Bridgeless Cuk Converter circuit during the positive cycle of the AC voltage source and the third switching cycle of the Cuk converter.

iii. Transfer Function

To analyze the converter, we apply the principle of average values under the assumption of periodic steady-state, where the average inductor voltage is $V_L = 0$. In this condition, we can state that $V_I = V_{S1}$ and $V_O = V_{S2}$. Applying Kirchhoff's Voltage Law (KVL) to the loop in Figure 5, we obtain:

$$\begin{aligned} V_{C1} - V_{S2} - V_{S1} &= 0 \\ V_{C1} - V_O - V_I &= 0 \\ V_{C1} &= V_O + V_I \end{aligned} \tag{1}$$

This shows that $V_{C1} > V_I$ and $V_{C1} > V_O$. Next, we analyze the converter operation in its two alternating cycles.

After steady-state operation begins, the Cuk converter cycles between stages 3 and 4 as described earlier. To derive the system's transfer function, we examine the inductor voltages V_{L1} and V_{L2} in each cycle. During

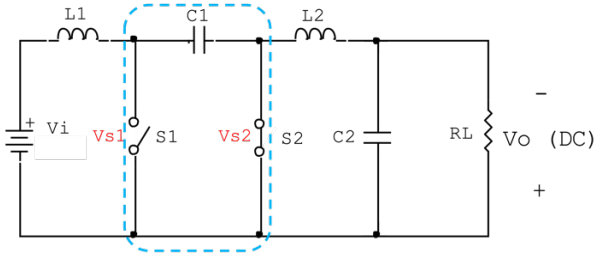

Figure 5: KVL analysis on S_1, C_1, and S_2.

cycle 3 (Figure 3(c)), when S_1 is on:

$$\begin{aligned} V_{L1} &= V_I \\ V_{L2} &= V_{C1} - V_O \end{aligned} \tag{2}$$

Since $V_{C1} > V_O$, we know V_{L2} is positive. During cycle 4 (Figure 3(d)), when S_1 is off:

$$\begin{aligned} V_{L1} &= V_I - V_{C1} \\ V_{L2} &= -V_O \end{aligned} \tag{3}$$

Because $V_{C1} > V_I$, the value of V_{L1} is negative in this cycle. The time-domain behavior of V_{L1} and V_{L2} is shown in Figures 6(b) and 6(c).

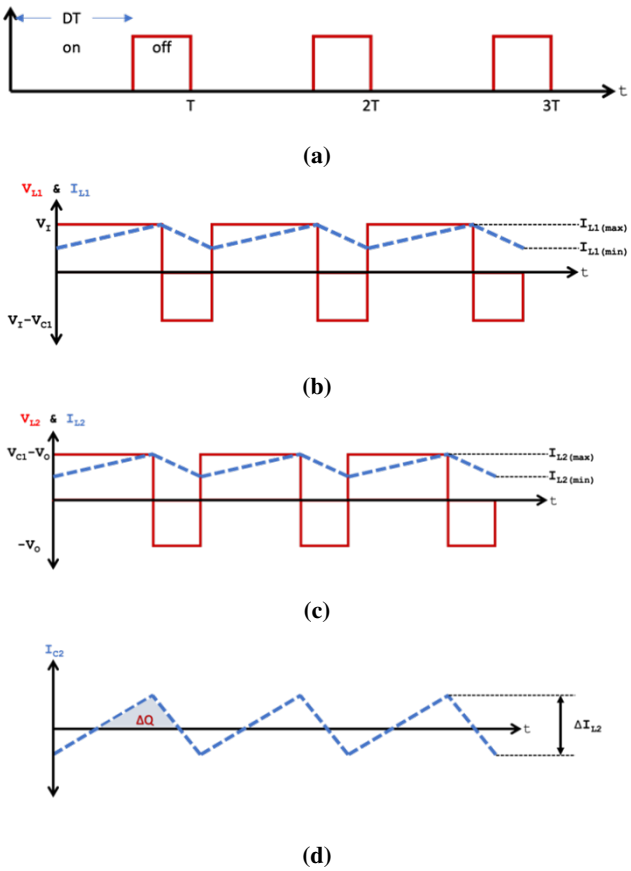

Figure 6: Time-domain diagrams: (a) V_{S1}; (b) V_{L1} and I_{L1}; (c) V_{L2} and I_{L2}; (d) I_{C2}.

As is known, the average inductor voltage V_L is zero over a complete switching cycle. Let T be the switching period and D be the duty cycle. By substituting Equations (2) and (3) into the average voltage expression for V_{L1}, we obtain:

$$\begin{aligned} \frac{1}{T}\left(DT \cdot V_{L1\_max} + (1-D)T \cdot V_{L1\_min}\right) &= 0 \\ D \cdot V_I + (1-D)(V_I - V_{C1}) &= 0 \\ V_I &= (1-D) \cdot V_{C1} \end{aligned} \tag{4}$$

Similarly, using the same principle for V_{L2} from the corresponding cycles:

$$\begin{aligned} \frac{1}{T}\left(DT \cdot V_{L2\_max} + (1-D)T \cdot V_{L2\_min}\right) &= 0 \\ D(V_{C1} - V_O) + (1-D)(-V_O) &= 0 \\ V_O &= D \cdot V_{C1} \end{aligned} \tag{5}$$

By combining Equations (4) and (5), the voltage transfer function of the system is obtained:

$$\frac{V_O}{V_I} = \frac{D}{1-D} \tag{6}$$

Assuming a 100% efficient system, power conservation gives $V_I I_I = V_O I_O$, leading to the current transfer function:

$$\frac{I_I}{I_O} = \frac{D}{1-D} \tag{7}$$

iv. Determination of Component Values

In transient conditions, referring again to Equation (2), and using the ripple of the input current $\Delta I_{L1} = I_{L1\_max} - I_{L1\_min}$, we have:

$$\begin{aligned} V_I &= L_1 \frac{di}{dt} = L_1 \cdot \Delta I_{L1} \cdot D \cdot T \\ L_1 &= \frac{V_I \cdot D}{\Delta I_{L1} \cdot f} \end{aligned} \tag{8}$$

where $f = \frac{1}{T}$ is the switching frequency. Similarly, using Equation (3) and defining $\Delta I_{L2} = I_{L2\_max} - I_{L2\_min}$:

$$\begin{aligned} -V_O &= L_2 \cdot \Delta I_{L2} \cdot (1-D) \cdot T \\ L_2 &= \frac{V_I \cdot D}{\Delta I_{L2} \cdot f} \end{aligned} \tag{9}$$

During the fourth cycle, capacitor C_1 is charged by current I_I, resulting in a voltage ripple ΔV_{C1}, which can be expressed as:

$$\Delta V_{C1} = \frac{I_I}{(1-D) \cdot f \cdot C_1} \tag{10}$$

Solving for C_1 and using $R_L = \frac{V_O}{I_O}$ and Equation (7):

$$C_1 = \frac{D \cdot V_O}{\Delta V_{C1} \cdot R_L \cdot f} \tag{11}$$

At the output stage, three components are connected: L_2, C_2, and R_L. The current flowing through capacitor C_2 is:

$$i_{C2} = i_{L2} - i_{RL} \tag{12}$$

Assuming $i_{L2} = \Delta I_{L2} + I_{L2}$ and that capacitors cannot pass DC current ($i_{RL} = I_{L2}$), Equation (12) becomes:

$$i_{C2} = \Delta I_{L2} \tag{13}$$

Using the capacitor charge-voltage relation $q = Cv$, we obtain the output voltage ripple ΔV_O:

$$\Delta V_O = \Delta Q / C_2 \tag{14}$$

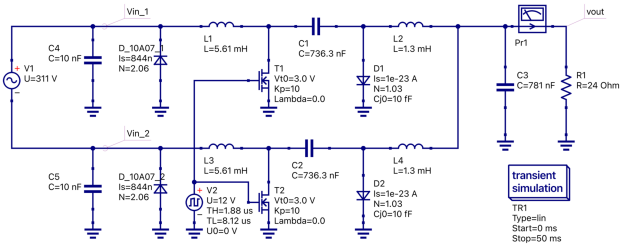

Figure 7: Cuk Converter circuit with values $L_1 = L_3$, $L_2 = L_4$, $C_1 = C_2 = C_3$, and $R_1 = R_L$ according to the design results.

Where the charge variation ΔQ is approximated by the area under i_{C2} from Figure 6(d), yielding:

$$\Delta Q = \frac{T \cdot \Delta I_{L2}}{8} \tag{15}$$

Substituting into Equation (14):

$$\Delta V_O = \frac{\Delta I_{L2}}{8 \cdot C_2 \cdot f} \tag{16}$$

Solving for C_2 using Equation (9) for ΔI_{L2}:

$$C_2 = \frac{V_I \cdot D}{\Delta V_O \cdot 8 \cdot L_2 \cdot f^2} \tag{17}$$

v. *Design of Cuk Converter*

Based on the specifications of the battery to be used and the required charger power, the design parameters for the bridgeless Cuk converter are determined as follows: the input voltage is $V_I(\text{AC}) = 220\ \text{V}_{\text{rms}} = 311\ \text{V}_{\text{peak}}$, the output voltage is $V_O(\text{DC}) = 72$ V, and the maximum output current is $I_O = 3$ A.

To calculate the minimum duty cycle using the peak input voltage:

$$\begin{aligned} D &= \frac{V_O}{V_I + V_O} \times 100\% \\ &= \frac{72}{311 + 72} \times 100\% = 18.8\% \end{aligned} \tag{18}$$

From the duty cycle, the maximum input current can be computed using Equation (7):

$$I_I = \frac{D}{1-D} \cdot I_O = \frac{0.188}{1 - 0.188} \cdot 3 = 0.695 \text{ A} \tag{19}$$

The load resistance is:

$$R_L = \frac{V_O}{I_O} = \frac{72}{3} = 24\ \Omega \tag{20}$$

The design parameters for ripple calculations are determined as follows. The output voltage ripple is set to $\Delta V_O = 1\% \cdot 72 = 0.72$ V, while the input current ripple is calculated as $\Delta I_{L1} = 15\% \cdot 0.695 = 104.25$ mA. The output current ripple is given by $\Delta I_{L2} = 15\% \cdot 3 = 450$ mA. For the capacitor voltage ripple, the chosen value is $\Delta V_{C1} = 2\% \cdot 72 + 311 = 7.66$ V. The switching frequency used in the design is $f = 100$ kHz.

Substituting these values into Equations (8), (9), (11), and (17), the component values are:

$$L_1 = \frac{V_I \cdot D}{\Delta I_{L1} \cdot f} = \frac{311 \cdot 0.188}{0.10425 \cdot 10^5} = 5.61 \text{ mH}$$

$$L_2 = \frac{V_O \cdot (1-D)}{\Delta I_{L2} \cdot f} = \frac{72 \cdot 0.812}{0.45 \cdot 10^5} = 1.3 \text{ mH}$$

$$C_1 = \frac{D \cdot V_O}{\Delta V_{C1} \cdot R_L \cdot f} = \frac{0.188 \cdot 72}{7.66 \cdot 24 \cdot 10^5} = 736.3 \text{ nF}$$

$$C_2 = \frac{V_O \cdot (1-D)}{8 \cdot L_2 \cdot f^2 \cdot \Delta V_O} = \frac{72 \cdot 0.812}{8 \cdot 1.3 \cdot 10^{-3} \cdot (10^5)^2 \cdot 0.72} = 781 \text{ nF}$$

The complete converter circuit with the selected components is shown in Figure 8.

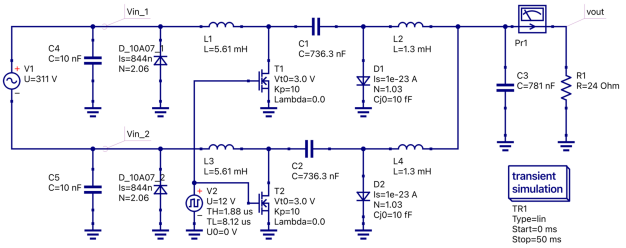

Figure 8: Circuit schematic of the bridgeless Cuk converter with selected components.

vi. *Selection of MOSFET and Diode as Electronic Switch*

In this study, switch S_1 will be implemented using a MOSFET, while S_2 will use a diode. The MOSFET experiences a relatively heavy workload.

Based on the third switching cycle (Figure 3(c)), the drain current is:

$$I_D = I_{S1} = I_I + I_O = 0.695 + 3 = 3.695 \text{ A} \quad (21)$$

The drain-source voltage during the fourth cycle (Figure 3(d)) is:

$$V_{DS} = V_{S1} = V_{C1} = V_O + V_I = 72 + 311 = 383 \text{ V} \quad (22)$$

Thus, the IRFP460 MOSFET is selected for S_1, which supports a maximum drain-source voltage of $V_{DS,\max} = 500$ V and a maximum drain current of $I_{D,\max} = 20$ A [24].

One advantage of the Cuk converter topology is that the source of the MOSFET is grounded, simplifying gate driving since it only needs to ensure $V_{GS} > V_{Th}$. Therefore, a low-side gate driver can be used.

For switch S_2, a diode with an ultra-fast recovery time is required to operate effectively at a switching frequency of 100 kHz. This diode must also handle the same voltage and current stress as S_1. The MUR1560 diode is selected, with a peak repetitive reverse voltage of $V_{RRM} = 600$ V, an average forward current of $I_{F(\text{AV})} = 15$ A, and a recovery time of 35–60 ns [25].

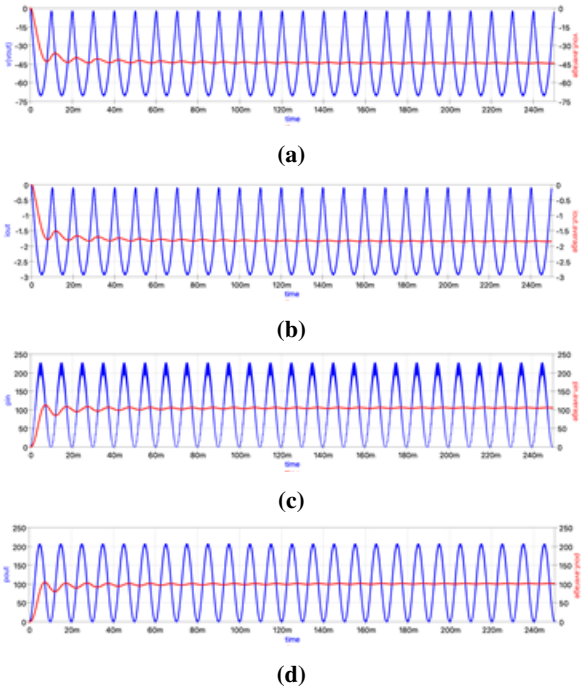

(a)

(b)

(c)

(d)

Figure 9: Output of the Cuk converter with a fixed duty cycle of 18.8%: (a) Peak voltage and average voltage; (b) Peak current and average current; (c) Input power and average input power; (d) Output power and average output power.

III. Results and Discussion

This section presents the simulation results and discussion of the designed bridgeless Cuk converter system. The performance of the converter is evaluated under two operating conditions: with a fixed duty cycle and with a feedback-controlled duty cycle, to assess its effectiveness in meeting the required output specifications.

i. Test Simulation with Fixed Duty Cycle

The circuit was simulated using QUCS-S 25.1 software [26]. Due to limitations in the available components within the simulation software, the key parameters of the IRFP460 MOSFET and MUR1560 diode were manually incorporated. The first simulation was conducted using a fixed duty cycle of 18.8%, which produced a fully rectified sinusoidal waveform.

The output voltage reaches a peak of $V_{\max} = -70.5$ V and has an average value of $V_{\text{avg}} = -45$ V. The load resistor (R_L) draws a peak current of $I_{\max} = -2.93$ A with an average of $I_{\text{avg}} = -1.87$ A, as shown in Figures 9(a) and 9(b).

The average input power is $P_{\text{in.avg}} = 105$ W and the average output power is $P_{\text{out.avg}} = 101$ W, shown in Figures 9(c) and 9(d). The converter efficiency is then calculated using:

$$\eta = \frac{P_{\text{out.avg}}}{P_{\text{in.avg}}} \times 100\% = \frac{101}{105} \times 100\% = 96.2\%$$

The peak voltage and current closely match the theoretical values and remain within the standard range specified by SNI 8928:2023 (67–78 V). However, since the output is a full-wave sinusoid, the average values of voltage and current do not yet conform to battery charging specifications.

ii. Test Simulation with Duty Cycle Control Feedback

The previous simulation produced an output resembling a full-wave signal. To achieve a more stable DC output, a feedback-controlled duty cycle was introduced. The duty cycle modulation is implemented using a comparator that compares a 100 kHz sawtooth waveform and the converter's output voltage, as shown in Figure 10(a).

Figures 10(b) and 10(c) display the sawtooth waveform and the resulting duty cycle modulation. The amplitude of the sawtooth signal was adjusted through a process of trial and error to meet two essential conditions: the duty cycle must remain greater than 0% when the output voltage reaches its maximum, and it must remain less than 100% when the output voltage is at its minimum.

This feedback system can be implemented using a voltage sensor, microcontroller, and PID control algorithm.

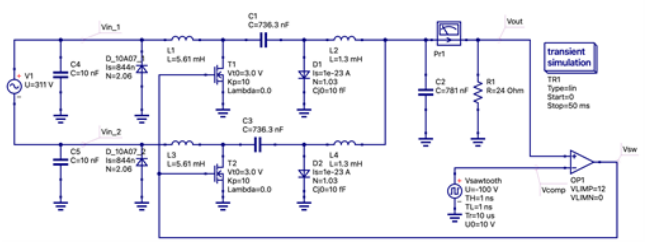

(a)

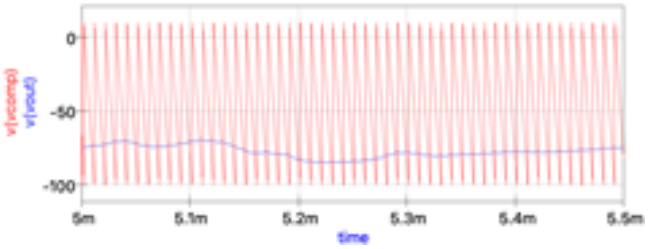

(b)

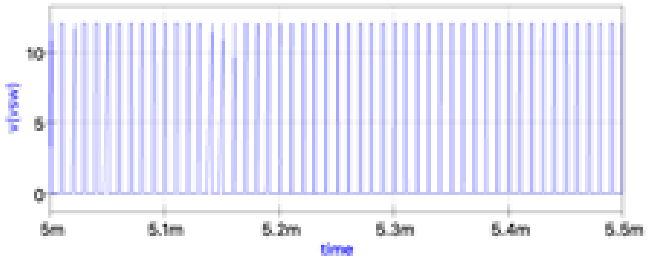

(c)

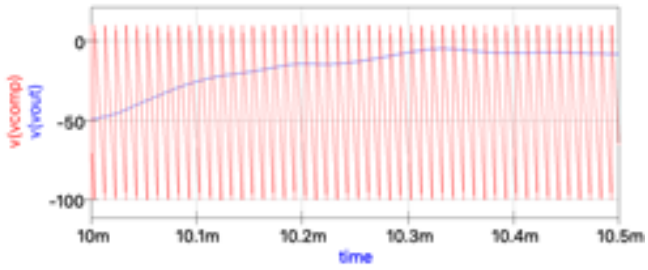

(d)

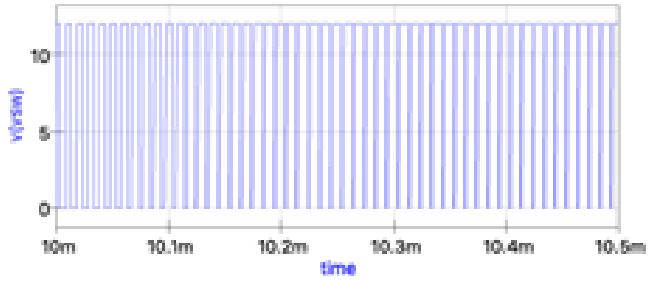

(e)

Figure 10: (a) Cuk Converter circuit with comparator as duty cycle feedback; (b) Comparison result between sawtooth signal and output voltage when the output voltage is at its highest, showing duty cycle $> 0\%$; (c) When the output voltage is at its lowest, showing duty cycle $< 100\%$.

The simulation shows the output voltage becomes more stable. The peak output voltage is $V_{\text{max}} = -100$ V, and the average is $V_{\text{avg}} = -73$ V. The output current peaks at $I_{\text{max}} = -4$ A, with an average of $I_{\text{avg}} = -3.05$ A (see Figures 11(a) and 11(b)).

The input power averages $P_{\text{in.avg}} = 233$ W and the output power is $P_{\text{out.avg}} = 226$ W, shown in Figures 11(c) and 11(d). The resulting efficiency is:

$$\eta = \frac{P_{\text{out.avg}}}{P_{\text{in.avg}}} \times 100\% = \frac{226}{233} \times 100\% = 96.99\%$$

Although the average voltage and current now meet the required specifications within a 5% tolerance, the peak voltage exceeds the SNI 8928:2023 standard and poses a safety risk for battery charging applications.

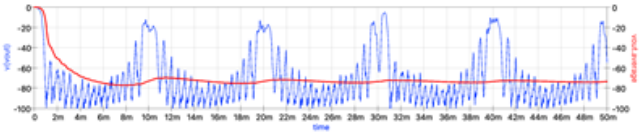

(a)

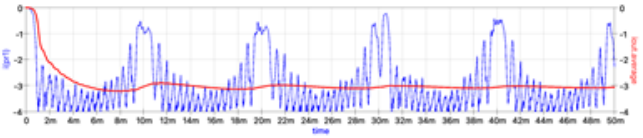

(b)

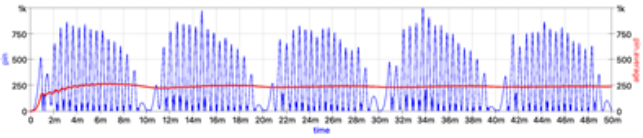

(c)

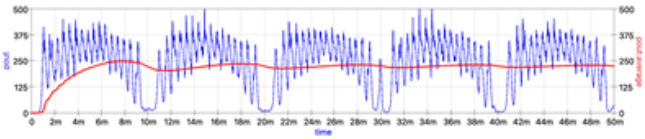

(d)

Figure 11: Output of the Cuk converter with duty cycle feedback (a) Peak voltage and average voltage (b) Peak current and average current (c) Input power and average input power (d) Output power and average output power

IV. Conclusion

Because the Cuk converter is essentially a DC-DC converter, applying a fixed duty cycle results in an output that mirrors the input waveform. As shown in the first simulation, calculating the duty cycle and component values based on battery specifications produces simulation results close to the theoretical peak values of V_{max} and I_{max}, but the output remains a full-wave sinusoidal shape, consistent with the AC input form. To address this issue, a duty cycle control system was introduced to stabilize the output voltage and current.

The Cuk converter is capable of increasing (boosting) or decreasing (bucking) the input voltage by adjusting the duty cycle. In the second simulation, the

addition of a duty cycle control mechanism resulted in average output values (V_{avg} and I_{avg}) that met the required specifications. However, several limitations were identified:

1. The comparator used for duty cycle control has suboptimal response. A better implementation would involve using a microcontroller with PID (proportional-integral-derivative) control.
2. Since the input of the bridgeless Cuk converter is single-phase AC, there are instants where the voltage and current drop to zero. Regardless of the duty cycle, the output during these intervals is also zero. This can be mitigated by using a three-phase AC input (polyphase) to the same converter topology.
3. The load used in the simulation is a purely resistive element, while actual battery charging requires different electrical characteristics. To protect and stabilize the output voltage and current, current feedback should also be implemented for dynamic duty cycle adjustment.

Acknowledgment

The author would like to thank Satya Wacana Christian University (UKSW) Salatiga for supporting this research through an internal grant with Research Contract No. 068/SPK-PP/RIK/08/2024.

References

[1] L. Ashok Kumar, S. Albert Alexander, and M. Rajendran, *DC–DC converter topologies for solar PV*. Elsevier, 2021, pp. 207–234. [Online]. Available: http://dx.doi.org/10.1016/b978-0-12-822730-5.00005-2

[2] R. W. Erickson, "Dc–DC Power Converters," *Wiley Encyclopedia of Electrical and Electronics Engineering*, jun 15 2007. [Online]. Available: http://dx.doi.org/10.1002/047134608X.W5808.PUB2

[3] F. Mocci and M. Tosi, "Comparison of power converter technologies in photovoltaic applications," in *Proceedings. Electrotechnical Conference Integrating Research, Industry and Education in Energy and Communication Engineering'*. IEEE, 1989, pp. 11–15. [Online]. Available: http://dx.doi.org/10.1109/MELCON.1989.49970

[4] M. Singh, M. R. Yadav, and D. K. Dhaked, "A Review on Various Voltage Boosting Topology in DC-DC Converter," *Recent Advances in Electrical & Electronic Engineering (Formerly Recent Patents on Electrical & Electronic Engineering)*, vol. 17, no. 6, pp. 554–572, 7 2024. [Online]. Available: http://dx.doi.org/10.2174/2352096516666230901140600

[5] N. Hanisah Baharudin, T. Muhammad Nizar Tunku Mansur, F. Abdul Hamid, R. Ali, and M. Irwanto Misrun, "Topologies of DC-DC Converter in Solar PV Applications," *Indonesian Journal of Electrical Engineering and Computer Science*, vol. 8, no. 2, p. 368, nov 1 2017. [Online]. Available: http://dx.doi.org/10.11591/IJEECS.V8.I2.PP368-374

[6] N. P. Besekar, "Dc-DC Converters Topology," *Journal of Image Processing and Intelligent Remote Sensing*, no. 32, pp. 11–21, feb 8 2023. [Online]. Available: http://dx.doi.org/10.55529/jipirs.32.11.21

[7] N. Raju, N. M. Mohan, and V. Kumar, *A Review of Extended Voltage Range DC-DC Converter Topologies*. Springer International Publishing, oct 21 2022, pp. 770–780. [Online]. Available: http://dx.doi.org/10.1007/978-3-031-19958-5_73

[8] V. Vaideeswaran, S. Bhuvanesh, and M. Devasena, "Battery Management Systems for Electric Vehicles using Lithium Ion Batteries," in *2019 Innovations in Power and Advanced Computing Technologies (i-PACT)*. IEEE, 3 2019, pp. 1–9. [Online]. Available: http://dx.doi.org/10.1109/i-PACT44901.2019.8959965

[9] V. Totev and V. Gueorgiev, "Batteries of Electric Vehicles," in *2021 13th Electrical Engineering Faculty Conference (BulEF)*. IEEE, sep 8 2021. [Online]. Available: http://dx.doi.org/10.1109/BulEF53491.2021.9690824

[10] R. M. Shahida, "Repurposing EV Batteries for Off-grid Homes," 2023.

[11] B. Dudić, "Global DEVELOPMENT AND SUSTAINABILITY OF LITHIUM-ION BATTERIES IN ELECTRIC VEHICLES," *Advanced Engineering Letters*, vol. 3, no. 2, pp. 83–90, 2024. [Online]. Available: http://dx.doi.org/10.46793/adeletters.2024.3.2.5

[12] V. Kumar and V. Jain, "Indepth analysis of the power management strategies in electric vehicles," *Energy Storage*, vol. 6, no. 2, 3 2024. [Online]. Available: http://dx.doi.org/10.1002/est2.611

[13] C. T., L. C. W. W., M. Z. E., R. L., P. Y., and A. B. N., "A Review on Recent Progress of Batteries for Electric Vehicles," 2019.

[14] J. B. Goodenough and M. H. Braga, "Batteries for electric road vehicles," *Dalton Transactions*, vol. 47, no. 3, pp. 645–648, 2018. [Online]. Available: http://dx.doi.org/10.1039/c7dt03026f

[15] N. S. Das, L. Padma Suresh, and S. Krishna Veni, "Materials and cell architecture of electric vehicle battery and its general parameters: A review," *Materials Today: Proceedings*, 2 2023. [Online]. Available: http://dx.doi.org/10.1016/j.matpr.2023.01.326

[16] Badan Standarisasi Nasional (BSN), "Sni 8928:2023 sistem baterai kendaraan bermotor listrik kategori l — spesifikasi baterai yang dapat ditukar untuk kendaraan motor listrik," 2023.

[17] B. Chandrasekar, C. Nallaperumal, and S. S. Dash, "A nonisolated three-port dc–dc converter with continuous input and output currents based on cuk topology for pv/fuel cell applications," *Electronics (Switzerland)*, vol. 8, no. 2, 2019. [Online]. Available: https://doi.org/10.3390/electronics8020214

[18] R. Pandey and B. Singh, "A cuk converter and resonant llc converter based e-bike charger for wide output voltage variations," *IEEE Transactions on Industry Applications*, vol. 57, no. 3, pp. 2682–2691, May 2021. [Online]. Available: https://doi.org/10.1109/TIA.2021.3066089

[19] S. Dutta, S. Gangavarapu, A. K. Rathore, R. K. Singh, S. K. Mishra, and V. Khadkikar, "Novel single-phase cuk-derived bridgeless pfc converter for on-board ev charger with reduced number of components," *IEEE Transactions on Industry Applications*, vol. 58,

no. 3, pp. 3999–4010, 2022. [Online]. Available: https://doi.org/10.1109/TIA.2022.3148969

[20] X. Lin, Z. Jin, F. Wang, and J. Luo, "A novel bridgeless cuk pfc converter with further reduced conduction losses and simple circuit structure," *IEEE Transactions on Industrial Electronics*, vol. 68, no. 11, pp. 10 699–10 708, Nov 2021. [Online]. Available: https://doi.org/10.1109/TIE.2020.3031527

[21] B. Singh and R. Kushwaha, "Ev battery charger with non-inverting output voltage-based bridgeless pfc cuk converter," *IET Power Electronics*, vol. 12, no. 13, pp. 3359–3368, Nov 2019. [Online]. Available: https://doi.org/10.1049/iet-pel.2019.0037

[22] R. Kushwaha and B. Singh, "A power quality improved ev charger with bridgeless cuk converter," *IEEE Transactions on Industry Applications*, pp. 5190–5203, Sep 2019. [Online]. Available: https://doi.org/10.1109/TIA.2019.2918482

[23] M. H. Rashid, *Power Electronics Handbook*. Butterworth-Heinemann, 2023. [Online]. Available: https://books.google.co.id/books?id=MIO3EAAAQBAJ

[24] Vishay Siliconix, "Irfp 460 - power mosfet," 2022. [Online]. Available: https://www.vishay.com/doc?91000

[25] On Semiconductor, "Mur1560 - switch-mode power rectifiers," 2014. [Online]. Available: http://onsemi.com

[26] M. E. Brinson and V. Kuznetsov, "Extended behavioural device modelling and circuit simulation with qucs-s," *International Journal of Electronics*, vol. 0, no. 0, pp. 1–14, 2017. [Online]. Available: https://doi.org/10.1080/00207217.2017.1357764